



## Abstract

Glyoxal and methylglyoxal are key products of oxidative photochemistry in the lower troposphere. Reliable measurements of such compounds are critical for testing our understanding of volatile organic compound (VOC) processing in this region. We present a new method for obtaining sensitive, high time resolution, in situ measurements of these compounds via laser-induced phosphorescent decays. By exploiting the unique phosphorescent lifetimes for each molecule, this method achieves speciation and high-sensitivity quantification of both molecules ( $3\sigma$  limits of detection of 11 ppt<sub>v</sub> in 5 min for glyoxal and 243 ppt<sub>v</sub> in 5 min for methylglyoxal). Additionally, this method enables the simultaneous measurement of both glyoxal and methylglyoxal using a single, non-wavelength-tunable light source, which will allow for the development of inexpensive and turnkey instrumentation. The simplicity and affordability of this new instrumentation would enable the construction of a long-term, spatially distributed database of these two key species. This chemical map can be used to constrain or drive regional or global models as well as provide verification of satellite observations.

## 1 Introduction

Glyoxal and methylglyoxal are nearly ubiquitous products of the HO<sub>x</sub>/NO<sub>x</sub> cycle (HO<sub>x</sub> = HO<sub>2</sub> + OH, NO<sub>x</sub> = NO<sub>2</sub> + NO), a photochemically driven oxidation process. This process, which oxidizes volatile organic compounds (VOCs) that are emitted by both anthropogenic and biogenic sources, has the potential to generate secondary organic aerosol (SOA) precursors and tropospheric ozone (O<sub>3</sub>). Both SOA and O<sub>3</sub> have been shown to have detrimental effects on human health and climate (Lippmann, 1991; Stieb et al., 2000; Lohmann, 2005; Isaksen et al., 2009). In an effort to understand these processes, observations of the VOC oxidation products, as well as the VOCs themselves, provide an important constraint for validating chemical models of the atmosphere by both driving these models as well as being a point of comparison and

AMTD

4, 6159–6183, 2011

### Quantification of gas-phase (methyl)glyoxal via the LIPGLOS method

S. B. Henry et al.

Title Page

Abstract

Introduction

Conclusions

References

Tables

Figures

⏪

⏩

◀

▶

Back

Close

Full Screen / Esc

Printer-friendly Version

Interactive Discussion





---

**Quantification of  
gas-phase  
(methyl)glyoxal via  
the LIPGLOS method**

---

S. B. Henry et al.

[Title Page](#)[Abstract](#)[Introduction](#)[Conclusions](#)[References](#)[Tables](#)[Figures](#)[⏪](#)[⏩](#)[◀](#)[▶](#)[Back](#)[Close](#)[Full Screen / Esc](#)[Printer-friendly Version](#)[Interactive Discussion](#)

as low as 170 ppt<sub>v</sub> per one minute) (Thalman and Volkamer, 2010). A similar spectroscopic method, incoherent broadband cavity enhanced absorption spectroscopy (IB-BCEAS), can achieve a 3σ LoD for glyoxal of 87 ppt<sub>v</sub> in 1 min (Washenfelder et al., 2008). Derivatization using DNPH-coated filters followed by HPLC analysis is a comparatively simple and inexpensive method of detection for both glyoxal (1.5 ppb<sub>v</sub> per four hours) and methylglyoxal (1.3 ppb<sub>v</sub> per four hours), but suffers from high detection limits, poor temporal resolution and potentially significant interferences (U.S. EPA, Center for Environmental Research Information, Research and Development, 1999; Ho and Yu, 2004).

In this study, we present the Laser-Induced Phosphorescence of (methyl)GLyOxal Spectrometry (LIPGLOS) method, a novel, sensitive, and relatively inexpensive method for measuring glyoxal and methylglyoxal that exploits the characteristic distribution of their phosphorescent photons with respect to time. We begin by describing the instrumental setup as well as data collection. We then discuss how the raw data is analyzed to retrieve glyoxal and methylglyoxal signals. The sensitivity is then characterized with a series of calibrations. To validate the concentrations observed by this method, simultaneous glyoxal calibrations of the LIPGLOS method and the Mad-LIP instrument was performed. Finally, an intercomparison of glyoxal data between the two methods during ambient sampling is examined.

## 2 Methods

### 2.1 Measurement principle

The relaxation of a population of excited molecules by any given pathway can be described by:

$$\frac{d[X^*]}{dt} = \frac{-1}{\tau}[X^*] \quad (1)$$

---

**Quantification of  
gas-phase  
(methyl)glyoxal via  
the LIPGLOS method**

---

S. B. Henry et al.

[Title Page](#)[Abstract](#)[Introduction](#)[Conclusions](#)[References](#)[Tables](#)[Figures](#)[⏪](#)[⏩](#)[◀](#)[▶](#)[Back](#)[Close](#)[Full Screen / Esc](#)[Printer-friendly Version](#)[Interactive Discussion](#)

The excited analyte is represented by  $[X^*]$ . The lifetime of the excited state,  $\tau$ , is unique to a specific species undergoing a particular relaxation pathway under a given set of conditions such as temperature, pressure, and in the case of luminescence, quantity of quenching molecules present. The solution to Eq. 1 is an exponential decay, with a decay constant of  $1/\tau$  and a prefactor of  $[X^*]_0$  (initial value of  $[X^*]$ ). During relaxation by luminescence, the intensity of the light emitted is directly proportional to  $[X^*]$ . Therefore, when a population of phosphorescing molecules is observed, the light will have the same temporal distribution as the excited state population; in this case, an exponential decay. If there are more than one phosphorescing species present, each with their own unique lifetime, the temporal distribution of photons is simply the sum of their exponential decays.

The fundamental difference between the LIPGLOS and Mad-LIP methods is how the photon-counting signal is used to derive concentrations. In the latter technique, signals are determined by integrating the phosphorescence signal over the entire decay interval (typically on the order of 10s of  $\mu$ s). As described in more detail below, differentiation of glyoxal and background signals via this technique requires dithering the wavelength of a tunable laser. In contrast, LIPGLOS utilizes the time-dependent decay of the phosphorescence signal to distinguish between these two molecules, allowing for speciation of both compounds at a single wavelength.

## 2.2 Experimental setup

The experimental setup was similar to that of the Mad-LIP instrument, which is described in detail elsewhere (Huisman et al., 2008). The primary differences were the light source as well as additional data collection protocols and hardware as detailed below. Included here is a brief description of the setup, which consists of the main components: light source, detection cell, data acquisition card, and cavity ringdown cell.

## 2.2.1 Light source

Two different light sources were utilized. The first source was a CW, fixed-wavelength diode laser (DL445-050-O, CrystaLaser) which emits 50 mW of 444.457 nm ( $\lambda_{CL}$ ) light with a nominal spectral bandwidth of 1 nm (FWHM) and a TEM<sub>00</sub> beam mode. An optional functionality was added by the manufacturer to allow turning the laser on and off by TTL logic. The laser transition time between the on and off states is <10 ns, effectively instantaneous for its application in these experiments. During operation, this laser was held on for 32  $\mu$ s, and turned off for the same duration which resulted in a repetition rate of 15 625 Hz.

The other light source was a custom tunable Ti:Sapphire laser (TU series, Photonics Industries International, Inc.), which was used to generate 440.104 nm ( $\lambda_{T:S,H}$ ) and 440.136 nm ( $\lambda_{T:S,L}$ ) light. The former was chosen because it is centered on a large, sharp (~0.06 nm wide) rovibrational absorption feature of glyoxal, and the latter is a nearby position that is off of the feature with an optical cross-section ~3 times lower. The optical cross-section of methylglyoxal is nearly identical (<0.2 % different) at either  $\lambda_{T:S,H}$  and  $\lambda_{T:S,L}$  which is ~10.2 and ~3.5 times smaller than the respective glyoxal optical cross-sections (Meller et al., 1991; Volkamer et al., 2005b). The laser operated at 3 kHz, an average power of 60 mW, and a bandwidth of <0.00078 nm.

## 2.2.2 Detection cell

The excitation light was aligned into a White-type multipass cell which allows for a longer absorption path length, thereby improving instrument sensitivity. The average light power directed into the cell was typically ~40 % of power emitted from the laser. For both lasers, this reduction in power was due to scatter/absorption by optics and two beam splitters: one to direct power to the cavity ringdown cell (Sect. 2.2.4) and another to a wavelength meter. An additional power loss unique to the CrystaLaser is incurred since it is operated with a duty cycle of 50 %, resulting in a factor of 2 power loss from its CW rated 50 mW. During operation, 32 passes are used through the volume of the cell which ambient air is drawn (~1/2 L). Phosphorescence photons were

### Quantification of gas-phase (methyl)glyoxal via the LIPGLOS method

S. B. Henry et al.

Title Page

Abstract

Introduction

Conclusions

References

Tables

Figures

⏪

⏩

◀

▶

Back

Close

Full Screen / Esc

Printer-friendly Version

Interactive Discussion





on-board memory buffer, allowing simultaneous data acquisition and communication of waveforms.

The entire data buffer, consisting of low hundreds of laser shots of data, was analyzed simultaneously. The arrival times of the photons were defined by the timestamp of an individual pulse which exceeds a specified threshold value for a specified amount of time. Once the period of integration was complete, a histogram was created from this list of arrival times. Additional instrumental diagnostics, such as temperature and pressure within the cell, were also recorded.

Due to equipment availability, a different digitizer card (Compuscope 14100-IM 14BIT, GaGe Applied Technologies) was used for ambient data acquisition. This possessed coarser, yet still adequate, time resolution (10 ns) with a duty cycle of ~48 % at 3 kHz. The lower duty cycle resulted from the data collection and transfer occurring on the card in series. To be comparable to the faster digitizer card from Alazar Technologies Inc., the integration time for the GaGe digitizer card is reported assuming it had a duty cycle of 100 % (e.g. 120 s of actual integration time will be reported as 57.6 s of comparable integration time).

## 2.2.4 Cavity Ringdown Spectroscopy

Instrumental calibrations were performed using Cavity Ringdown Spectroscopy (CRDS), an absolute quantification method in that it relies only on well-documented absorption cross-sections. Further details about the theory of this method is described elsewhere (O'Keefe and Deacon, 1988).

A cavity 62 cm long and 0.635 cm in diameter was formed between two parallel, highly reflective mirrors with a radius of curvature of 1 m (99.995 % reflectance) (901-0010-0440, Los Gatos Research Inc.). The bulk of the cavity was encased in a 3/8" O.D., 1/4" I.D. PTFE tube. Halfway along the cavity, a PTFE tee was used as an inlet for calibrant gas. On each end of the cavity, the mirror mounts were coupled via metal bellows to a Teflon PTFE tee which coupled the cell to exhausts ports for the cell. The dead volumes between the exhaust ports and the mirrors were flushed with zero

## Quantification of gas-phase (methyl)glyoxal via the LIPGLOS method

S. B. Henry et al.

Title Page

Abstract

Introduction

Conclusions

References

Tables

Figures

⏪

⏩

◀

▶

Back

Close

Full Screen / Esc

Printer-friendly Version

Interactive Discussion





## Quantification of gas-phase (methyl)glyoxal via the LIPGLOS method

S. B. Henry et al.

Title Page

Abstract

Introduction

Conclusions

References

Tables

Figures

⏪

⏩

◀

▶

Back

Close

Full Screen / Esc

Printer-friendly Version

Interactive Discussion



air (Airgas, Inc.) through a 200 SCCM flow controller (1779A, MKS Instruments) to prevent optics fouling as well as bias. This purging did not allow any sample gas to mix beyond the exhaust ports, fixing the physical absorber path length to 42 cm. This cell design is based on to the instrument described by Brown et al. (2002). The entire cavity length between, and including, the exhaust tee fittings was enclosed in a 1.5'' by 1.5'' block of aluminum which was maintained at a constant temperature (~35°C) to discourage analyte deposition inside the cavity.

A 10 SCCM flow controller (1779A, MKS Instruments) supplied calibrant gas that was then diluted by zero air (Airgas, Inc.). The zero air was delivered by a 200 SCCM flow controller (1779A, MKS Instruments) at a rate which made up the remainder to a total flow of 100 SCCM of diluted calibrant. The purge was held at 100 SCCM using a 200 SCCM flow controller (1779A, MKS Instruments). To maintain a constant cell pressure and therefore achieve a stable baseline, both the purge and the diluted calibrant flows were held constant.

Laser pulses were introduced into the cavity through one of the high-reflectivity mirror. With each reflection, a small quantity of light escaped through the mirrors. On the opposite side of this cavity, a PMT (H5783, Hamamatsu), guarded by a 440 nm bandpass filter, detected this escaped light. Loss of photons within the cavity is a first-order process, thus the light leaking from the cavity has the characteristics of an exponential decay. The loss of light within the cavity, whether the light is absorbed by a chemical, transmitted through/absorbed by the mirrors, or scattered by gas/aerosols, can be quantified by the decay lifetime,  $\tau$ . The number density of a chemical absorber (molecules  $\text{cm}^{-3}$ ) can be determined by relating two determined lifetimes, those determined with and without the presence of the absorber, by the following equation:

$$N_d = \frac{1-R}{\sigma \ell_a} \left( \frac{\tau_o - \tau}{\tau} \right) \quad (2)$$

where  $N_d$  is the number density of the absorber,  $R$  is mirror reflectivity,  $\sigma$  is the absorption cross-section,  $\ell_a$  is the pathlength of the absorber,  $\tau$  and  $\tau_o$  are the lifetimes with and without the absorber, respectively (Zalicki and Zare, 1994).

### 3 Data and signal characterization

#### 3.1 Analysis

The collected histogram includes several sources of photons: laser scatter, fluorescence of cell walls and gas-phase species, and phosphorescence. Since the laser scatter and fluorescence are both short-lived compared to phosphorescence, fitting was performed after 2.5  $\mu\text{s}$  to eliminate their influence on the measurement and was continued until no more data was recorded, as in the case of the Ti:Sapphire (45  $\mu\text{s}$ , Fig. 1a), or until the laser was turned back on, as with the CrystaLaser (35  $\mu\text{s}$ , Fig. 1b). Due to this gated temporal selectivity, this method does not suffer from interference from unfiltered ambient air at 60% relative humidity or  $\text{NO}_2$  fluorescence (Huisman et al., 2008). This, however, does not eliminate signal from dark counts or stray ambient light. These two contributions are manifested as time independent background.

Histograms collected from a mixture of glyoxal and methylglyoxal, such as in ambient air, are a linear combination of exponential decays with the respective characteristic lifetimes for glyoxal and methylglyoxal. These lifetimes were determined individually via a series of laboratory calibrations. The decays during these calibrations were fit using an iterative least squares algorithm to Eq. (3):

$$D(t) = Ae^{-t/\tau} + B \quad (3)$$

Where  $A$  is the prefactor,  $t$  is time,  $\tau$  is the phosphorescent lifetime, and  $B$  is the background. Example decays from the glyoxal and methylglyoxal calibrations are shown in Fig. 2. The  $\tau$  for glyoxal and methylglyoxal was determined in air at 100 Torr to be  $12.75_3 \pm 0.08 \mu\text{s}$  and  $7.26_3 \pm 0.03 \mu\text{s}$ , respectively. Once these lifetimes were established, collected decays were then fit to Eq. (4) using the least squares method:

$$D(t) = A_{\text{gly}}e^{-t/\tau_{\text{gly}}} + A_{\text{mgly}}e^{-t/\tau_{\text{mgly}}} + B \quad (4)$$

## Quantification of gas-phase (methyl)glyoxal via the LIPGLOS method

S. B. Henry et al.

Title Page

Abstract

Introduction

Conclusions

References

Tables

Figures

⏪

⏩

◀

▶

Back

Close

Full Screen / Esc

Printer-friendly Version

Interactive Discussion



where  $\tau_x$  is the phosphorescent lifetime of the analyte which was determined in the previously mentioned experiments,  $A_x$  is the magnitude of the analyte, and  $B$  is the background.

The nature of data collection and the analysis permits two distinct methods of averaging: fitting the decays followed by averaging the prefactors (prefactor averaging), or fitting to an averaged decay (decay averaging). To determine the performance of each method, a constant concentration was sampled for two hours at one minute integration. Figure 3a demonstrates how the relative error changes with averaging bin size for both methods. The near unity slope in the line of best fit in Fig. 3b between the relative errors of the two methods taken at the different bin sizes illustrates that they have the same behavior.

### 3.2 Calibration

Glyoxal and methylglyoxal calibrant gases were synthesized from glyoxal trimer dihydrate (G680-5, Sigma-Aldrich) and 40 wt % aqueous pyruvaldehyde solution (w296902, Sigma-Aldrich) as described elsewhere (Kroll et al., 2005; Galloway et al., 2009). The gases were stored in separate 12 L glass bulbs at a concentration of  $\sim 1\%$  with a balance gas of  $N_2$ . Approximately  $2\text{ cm}^3$  of this gas was transferred to a stainless steel cylinder with an inner surface prepared with a fluorinated polymer solution (PFC 802A, FluoroPel) to minimize wall loss. We have empirically determined that calibrant concentrations in these containers are stable for months.

Once the standard gas was characterized via CRDS (see Sect. 2.2.4), independent phosphorescent calibrations were performed for glyoxal and methylglyoxal by flowing multiple concentrations (low ppt<sub>v</sub> to low ppb<sub>v</sub>) of the calibrant gases through the detection cell. The calibrant gas flow was controlled using a 10 SCCM flow controller (1779A, MKS Instruments), diluted with  $\sim 20$  SLM zero air (Airgas, Inc.) through a 100 SLM flow controller (1559A, MKS Instruments) and introduced into the LIP detection cell. Table 1 summarizes the calibration curves resulting from these experiments.

## Quantification of gas-phase (methyl)glyoxal via the LIPGLOS method

S. B. Henry et al.

Title Page

Abstract

Introduction

Conclusions

References

Tables

Figures

⏪

⏩

◀

▶

Back

Close

Full Screen / Esc

Printer-friendly Version

Interactive Discussion





cycle of the LIPGLOS method. Values obtained via LIPGLOS were cross-calibrated with the Mad-LIP instrument, which itself was calibrated in the fashion described elsewhere (Huisman et al., 2008). During the morning of the 21st when concentrations are the lowest, the standard deviation of the LIPGLOS and Mad-LIP data is 4.2 ppt<sub>v</sub> (extrapolated) and 2.9 ppt<sub>v</sub> in 40 s, respectively. This LIPGLOS precision error in the night time ambient data corresponds to a 5 min 3 $\sigma$  LoD (4.6 ppt<sub>v</sub>) which is lower than what was calculated during the calibrations (11 ppt<sub>v</sub>). Furthermore, this LIPGLOS LoD would be an upper limit as the precision error during that period incorporates some diurnal variation.

## 5 Conclusions

We have developed a method exploiting the difference in phosphorescent lifetimes of glyoxal and methylglyoxal to allow their simultaneous quantification in ambient air at a single wavelength. Speciation of composite signals is performed by fitting ambient phosphorescent decays to a linear combination of decays with known characteristic phosphorescent lifetimes established from laboratory experiments.

This method achieves atmospherically relevant 3 $\sigma$  limits of detection, the lowest of which were 11 ppt<sub>v</sub> glyoxal in five minutes at  $\lambda_{T:S,H}$  (440.104 nm, at the maximum of an absorption feature) and 243 ppt<sub>v</sub> methylglyoxal in five minutes at  $\lambda_{T:S,L}$  (440.136 nm). Ambient data in Madison, WI showed that glyoxal concentrations as determined by the LIPGLOS method when compared to those achieved via the Mad-LIP instrument had a slope of 0.98 and a correlation coefficient of 0.87.

A major advantage of LIPGLOS over the Mad-LIP instrument is that it does not require a tunable light source. This allows the use of simpler light sources, including high powered LEDs or laser diodes, which results in less expensive, lighter, more compact, more robust field instrumentation. Assuming a laser repetition rate of 20 kHz, using all available 50 mW for detection, a laser pulse width of 35 ns, and glyoxal and methylglyoxal cross sections at  $\lambda_{T:S,H}$ , the projected 5 min 3 $\sigma$  limits of detection are 1.9 ppt<sub>v</sub> for

## Quantification of gas-phase (methyl)glyoxal via the LIPGLOS method

S. B. Henry et al.

Title Page

Abstract

Introduction

Conclusions

References

Tables

Figures

◀

▶

◀

▶

Back

Close

Full Screen / Esc

Printer-friendly Version

Interactive Discussion



---

**Quantification of  
gas-phase  
(methyl)glyoxal via  
the LIPGLOS method**

---

S. B. Henry et al.

[Title Page](#)[Abstract](#)[Introduction](#)[Conclusions](#)[References](#)[Tables](#)[Figures](#)[⏪](#)[⏩](#)[◀](#)[▶](#)[Back](#)[Close](#)[Full Screen / Esc](#)[Printer-friendly Version](#)[Interactive Discussion](#)

glyoxal and 55 ppt<sub>v</sub> for methylglyoxal. Alternatively, one can select a laser wavelength that, rather than optimized for glyoxal, is optimized to achieve similar sensitivities for both species. This would decrease the glyoxal interference in the methylglyoxal signal by choosing a wavelength of reduced glyoxal absorption, thereby decreasing the glyoxal sensitivity. Keeping previously assumed improvement parameters except using the wavelength 436.027 nm, where glyoxal and methylglyoxal cross-sections are  $1.11 \times 10^{-19} \text{ cm}^2 \text{ molecule}^{-1}$ , the projected limits of detection are 17 ppt<sub>v</sub> for glyoxal and 50 ppt<sub>v</sub> for methylglyoxal.

This method permits instrumentation both easy to operate and inexpensively produced, primarily due to the simple and inexpensive light source. Deployment of such instrumentation at established measurement sites would create a spatially detailed map of glyoxal and methylglyoxal, useful for either driving or as a comparison to regional-scale chemical models, as well as validation for satellite instruments. A candidate for such potential sites include the EPA atmospheric monitoring stations maintained all over the US that continuously measure particulate matter, NO<sub>2</sub>, CO, and O<sub>3</sub>, all of which are also tied to oxidative chemistry. The effect of transport between urban and rural areas on oxidation chemistry could be captured in this spatially detailed database of glyoxal and methylglyoxal concentrations.

*Acknowledgements.* The authors would like to thank Josh DiGangi for help with signal analysis. This work was funded by the L'Oréal USA Fellowships for Women in Science program.

## References

- Brown, S. S., Stark, H., Ciciora, S. J., McLaughlin, R. J., and Ravishankara, A. R.: Simultaneous in situ detection of atmospheric NO<sub>3</sub> and N<sub>2</sub>O<sub>5</sub> via cavity ring-down spectroscopy, *Rev. Sci. Instrum.*, 73, 3291–3301, 2002. 6167
- Fu, T.-M., Jacob, D. J., Wittrock, F., Burrows, J., Vrekoussis, M., and Henze, D.: Global budgets of atmospheric glyoxal and methylglyoxal, and implications for formation of secondary organic aerosols, *J. Geophys. Res.*, 113, D15303, 2008. 6161

---

**Quantification of  
gas-phase  
(methyl)glyoxal via  
the LIPGLOS method**

---

S. B. Henry et al.

[Title Page](#)[Abstract](#)[Introduction](#)[Conclusions](#)[References](#)[Tables](#)[Figures](#)[⏪](#)[⏩](#)[◀](#)[▶](#)[Back](#)[Close](#)[Full Screen / Esc](#)[Printer-friendly Version](#)[Interactive Discussion](#)

- Galloway, M. M., Chhabra, P. S., Chan, A. W. H., Surratt, J. D., Flagan, R. C., Seinfeld, J. H., and Keutsch, F. N.: Glyoxal uptake on ammonium sulphate seed aerosol: reaction products and reversibility of uptake under dark and irradiated conditions, *Atmos. Chem. Phys.*, 9, 3331–3345, doi:10.5194/acp-9-3331-2009, 2009. 6169
- 5 Guenther, A., Hewitt, C., Erickson, D., Fall, R., Geron, C., Graedel, T., Harley, P., Klinger, L., Lerdau, M., McKay, W., Pierce, T., Scholes, B., Steinbrecher, R., Tallamaraju, R., Taylor, J., and Zimmerman, P.: A global model of natural volatile organic-compound emissions, *J. Geophys. Res.-Atmos.*, 100, 8873–8392, 1995. 6161
- 10 Hallquist, M., Wenger, J. C., Baltensperger, U., Rudich, Y., Simpson, D., Claeys, M., Dommen, J., Donahue, N. M., George, C., Goldstein, A. H., Hamilton, J. F., Herrmann, H., Hoffmann, T., Iinuma, Y., Jang, M., Jenkin, M. E., Jimenez, J. L., Kiendler-Scharr, A., Maenhaut, W., McFiggans, G., Mentel, Th. F., Monod, A., Prévôt, A. S. H., Seinfeld, J. H., Surratt, J. D., Szmigielski, R., and Wildt, J.: The formation, properties and impact of secondary organic aerosol: current and emerging issues, *Atmos. Chem. Phys.*, 9, 5155–5236, doi:10.5194/acp-9-5155-2009, 2009. 6161
- 15 Ho, S. S. H. and Yu, J. Z.: Determination of airborne carbonyls: Comparison of a thermal desorption/GC method with the standard DNPH/HPLC method, *Environ. Sci. Technol.*, 38, 862–870, 2004. 6162
- Huisman, A. J., Hottle, J. R., Coens, K. L., DiGangi, J. P., Galloway, M. M., Kammrath, A., and Keutsch, F. N.: Laser-induced phosphorescence for the in situ detection of glyoxal at part per trillion mixing ratios, *Anal. Chem.*, 80, 5884–5891, 2008. 6161, 6163, 6165, 6168, 6172
- 20 Isaksen, I. S. A., Granier, C., Myhre, G., Berntsen, T. K., Dalsøren, S. B., Gauss, M., Klimont, Z., Benestad, R., Bousquet, P., Collins, W., Cox, T., Eyring, V., Fowler, D., Fuzzi, S., Jöckel, P., Laj, P., Lohmann, U., Maione, M., Monks, P., Prevot, A. S. H., Raes, F., Richter, A., Rognerud, B., Schulz, M., Shindell, D., Stevenson, D. S., Storelvmo, T., Wang, W. C., van Weele, M., Wild, M., and Wuebbles, D.: Atmospheric composition change: Climate-Chemistry interactions, *Atmos. Environ.*, 43, 5138–5192, 2009. 6160
- 25 Kroll, J. H., Ng, N. L., Murphy, S. M., Varutbangkul, V., Flagan, R. C., and Seinfeld, J. H.: Chamber studies of secondary organic aerosol growth by reactive uptake of simple carbonyl compounds, *J. Geophys. Res.-Atmos.*, 110, D23207, 2005. 6169
- 30 Lippmann, M.: Health effects of tropospheric ozone, *Environ. Sci. Technol.*, 25, 1954–1962, 1991. 6160
- Lohmann, U. and Feichter, J.: Global indirect aerosol effects: a review, *Atmos. Chem. Phys.*, 5,



**Quantification of  
gas-phase  
(methyl)glyoxal via  
the LIPGLOS method**

S. B. Henry et al.

Title Page

Abstract

Introduction

Conclusions

References

Tables

Figures

◀

▶

◀

▶

Back

Close

Full Screen / Esc

Printer-friendly Version

Interactive Discussion



715–737, doi:10.5194/acp-5-715-2005, 2005. 6160

Meller, R., Raber, W., Crowley, J. N., Jenkin, M. E., and Moortgat, G. K.: The UV-visible absorption spectrum of methylglyoxal, *J. Photoch. Photobio. A*, 62, 163–171, 1991. 6164

O’Keefe, A. and Deacon, D. A. G.: Cavity Ring-down Optical Spectrometer for Absorption-Measurements Using Pulsed Laser Sources, *Rev. Sci. Instrum.*, 59, 2544–2551, 1988. 6166

Sinreich, R., Coburn, S., Dix, B., and Volkamer, R.: Ship-based detection of glyoxal over the remote tropical Pacific Ocean, *Atmos. Chem. Phys.*, 10, 11359–11371, doi:10.5194/acp-10-11359-2010, 2010. 6161

Spaulding, R. S., Schade, G. W., Goldstein, A. H., and Charles, M. J.: Characterization of secondary atmospheric photooxidation products: Evidence for biogenic and anthropogenic sources, *J. Geophys. Res.-Atmos*, 108, D4247, 2003. 6161

Stieb, D. M., Beveridge, R. C., Brook, J. R., Smith-Doiron, M., Burnett, R. T., Dales, R. E., Beaulieu, S., Judek, S., and Mamedov, A.: Air pollution, aeroallergens and cardiorespiratory emergency department visits in Saint John, Canada, *J. Expo. Anal. Env. Epid.*, 10, 461–477, 2000. 6160

Thalman, R. and Volkamer, R.: Inherent calibration of a blue LED-CE-DOAS instrument to measure iodine oxide, glyoxal, methyl glyoxal, nitrogen dioxide, water vapour and aerosol extinction in open cavity mode, *Atmos. Meas. Tech.*, 3, 1797–1814, doi:10.5194/amt-3-1797-2010, 2010. 6162

Turro, N. J. and Engel, R.: Quenching of Biacetyl Fluorescence and Phosphorescence, *J. Am. Chem. Soc.*, 91, 7113–7121, 1969. 6170

U.S. EPA, Center for Environmental Research Information, Research and Development: Compendium of Methods for the Determination of Toxic Organic Compounds in Ambient Air, TO-11A, Center for Environmental Research Information, National Risk Management Laboratory, Office of Research and Development, U.S. EPA, Cincinnati, OH, 2 Edn., 1999. 6162

Volkamer, R., Molina, L. T., Molina, M. J., Shirley, T., and Brune, W. H.: DOAS measurement of glyoxal as an indicator for fast VOC chemistry in urban air, *Geophys. Res. Lett.*, 32, L08806, 2005a. 6161

Volkamer, R., Spietz, P., Burrows, J., and Platt, U.: High-resolution absorption cross-section of glyoxal in the UV-vis and IR spectral ranges, *J. Photoch. Photobio. A*, 172, 35–46, 2005b. 6164

Volkamer, R., San Martinti, F., Molina, L. T., Salcedo, D., Jimenez, J., and Molina, M. J.: A missing sink for gas-phase glyoxal in Mexico City: Formation of secondary organic aerosol,

---

**Quantification of  
gas-phase  
(methyl)glyoxal via  
the LIPGLOS method**

S. B. Henry et al.

---

Title Page

Abstract

Introduction

Conclusions

References

Tables

Figures

⏪

⏩

◀

▶

Back

Close

Full Screen / Esc

Printer-friendly Version

Interactive Discussion



Geophys. Res. Lett., 34, doi:10.1029/2007GL030752, 2007. 6161

Vrekoussis, M., Wittrock, F., Richter, A., and Burrows, J. P.: Temporal and spatial variability of glyoxal as observed from space, *Atmos. Chem. Phys.*, 9, 4485–4504, 2009, <http://www.atmos-chem-phys.net/9/4485/2009/>. 6161

5 Vrekoussis, M., Wittrock, F., Richter, A., and Burrows, J. P.: GOME-2 observations of oxygenated VOCs: what can we learn from the ratio glyoxal to formaldehyde on a global scale?, *Atmos. Chem. Phys.*, 10, 10145–10160, doi:10.5194/acp-10-10145-2010, 2010. 6161

Washenfelder, R. A., Langford, A. O., Fuchs, H., and Brown, S. S.: Measurement of glyoxal using an incoherent broadband cavity enhanced absorption spectrometer, *Atmos. Chem. Phys.*, 8, 7779–7793, doi:10.5194/acp-8-7779-2008, 2008. 6162

10 Wittrock, F., Richter, A., Oetjen, H., Burrows, J., Kanakidou, M., Myriokefalitakis, S., Volkamer, R., Beirle, S., Platt, U., and Wagner, T.: Simultaneous global observations of glyoxal and formaldehyde from space, *Geophys. Res. Lett.*, 33, doi:10.1029/2006GL026310, 2006. 6161

15 Yu, G., Bayer, A. R., Galloway, M. M., Korshavn, K. J., Fry, C., and Keutsch, F. N.: Glyoxal and methylglyoxal in aqueous ammonium sulfate solutions: products, kinetics and hydration effects, *Environ. Sci. Technol.*, submitted, 2011. 6161

Zalicki, P. and Zare, R. N.: Cavity ring-down spectroscopy for quantitative absorption measurements, *J. Chem. Phys.*, 102, 2708–2717, 1994. 6167

## Quantification of gas-phase (methyl)glyoxal via the LIPGLOS method

S. B. Henry et al.

**Table 1.** Summary of the results from the six different calibrations with only either glyoxal or methylglyoxal present inside the detection cell. All data presented here is 5 min integration. Data taken at  $\lambda_{\text{CL}}$  has been scaled from 15 min integration to 5 min for purpose of comparison. For purposes of comparison, Mad-LIP has an extrapolated  $3\sigma$  LoD of 1 ppt<sub>v</sub> per 5 min.

Species	$\lambda$	$\sigma$ (cm <sup>2</sup> molecule <sup>-1</sup> )	Sensitivity (prefactor ppt <sub>v</sub> <sup>-1</sup> mW <sup>-1</sup> )	Intercept (prefactor ppt <sub>v</sub> <sup>-1</sup> mW <sup>-1</sup> )	$R^2$	$3\sigma$ LoD (ppt <sub>v</sub> )
Glyoxal	T:S,H	$10.20 \times 10^{-19}$	$(1.5_0 \pm 0.1) \times 10^{-2}$	$-0.4_0 \pm 0.3$	0.991	11
	T:S,L	$3.42 \times 10^{-19}$	$(4.0_0 \pm 0.2) \times 10^{-3}$	$-0.4_5 \pm 0.1$	0.996	37
	CL	$1.05 \times 10^{-19}$	$(3.59_8 \pm 0.07) \times 10^{-4}$	$0.04_8 \pm 0.01$	0.999	146
Methylglyoxal	T:S,H	$1.00 \times 10^{-19}$	$(6.30_8 \pm 0.07) \times 10^{-4}$	$1.79_4 \pm 0.02$	1.000	322
	T:S,L	$1.00 \times 10^{-19}$	$(6.8_4 \pm 0.3) \times 10^{-4}$	$1.78_8 \pm 0.08$	0.996	269
	CL	$0.96 \times 10^{-19}$	$(1.5_4 \pm 0.1) \times 10^{-4}$	$0.04_2 \pm 0.02$	0.991	243

Title Page

Abstract

Introduction

Conclusions

References

Tables

Figures

⏪

⏩

◀

▶

Back

Close

Full Screen / Esc

Printer-friendly Version

Interactive Discussion

## Quantification of gas-phase (methyl)glyoxal via the LIPGLOS method

S. B. Henry et al.

**Table 2.** Summary of the results from the six different calibrations with both glyoxal and methylglyoxal present inside the detection cell. The last column represents the relative percent difference in sensitivities as determined in a pure calibration versus in a mixture ( $100 \times (\text{Sensitivity}_{\text{mixed}} - \text{Sensitivity}_{\text{pure}}) / \text{Sensitivity}_{\text{pure}}$ ).

Species	$\lambda$	Sensitivity (prefactor $\text{ppt}_v^{-1} \text{ mW}^{-1}$ )	Intercept (prefactor $\text{ppt}_v^{-1} \text{ mW}^{-1}$ )	$R^2$	Sensitivity Difference (%)
Glyoxal	T:S,H	$(1.27_3 \pm 0.07) \times 10^{-2}$	$-0.1_8 \pm 0.2$	0.977	-15.1
	T:S,L	$(3.7_9 \pm 0.1) \times 10^{-3}$	$-0.43_5 \pm 0.07$	0.989	-5.3
	CL	$(2.8_9 \pm 0.4) \times 10^{-4}$	$-0.05_8 \pm 0.09$	0.905	-19.7
Methyl- glyoxal	T:S,H	$(2.5 \pm 3) \times 10^{-4}$	$0.4_2 \pm 0.4$	0.064	-60.3
	T:S,L	$(5.2 \pm 1) \times 10^{-4}$	$1.2_8 \pm 0.2$	0.539	-24.0
	CL	$(1.5_2 \pm 0.2) \times 10^{-4}$	$0.07_2 \pm 0.06$	0.944	-1.3

Title Page

Abstract

Introduction

Conclusions

References

Tables

Figures

◀

▶

◀

▶

Back

Close

Full Screen / Esc

Printer-friendly Version

Interactive Discussion

**Quantification of  
gas-phase  
(methyl)glyoxal via  
the LIPGLOS method**

S. B. Henry et al.

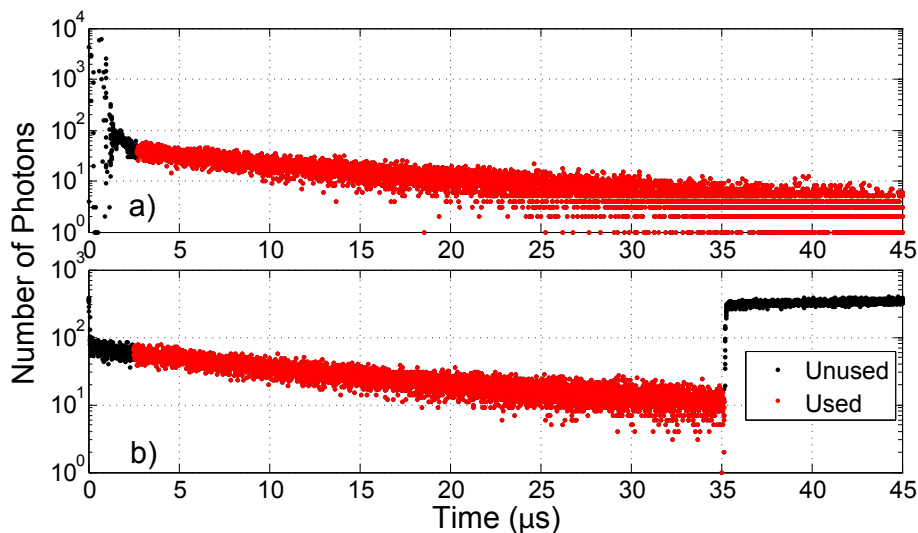


**Fig. 1.** (a) Example histogram corresponding to 1000 ppt<sub>v</sub> glyoxal collected with Ti:Sapphire laser in 5 min. The initial large peak is the laser pulse. (b) Example histogram corresponding to 4200 ppt<sub>v</sub> glyoxal collected with CrystaLaser in 15 min. Both the initial peak as well as the plateau after the used data results from laser scatter.

[Title Page](#)[Abstract](#)[Introduction](#)[Conclusions](#)[References](#)[Tables](#)[Figures](#)[◀](#)[▶](#)[◀](#)[▶](#)[Back](#)[Close](#)[Full Screen / Esc](#)[Printer-friendly Version](#)[Interactive Discussion](#)

**Quantification of  
gas-phase  
(methyl)glyoxal via  
the LIPGLOS method**

S. B. Henry et al.

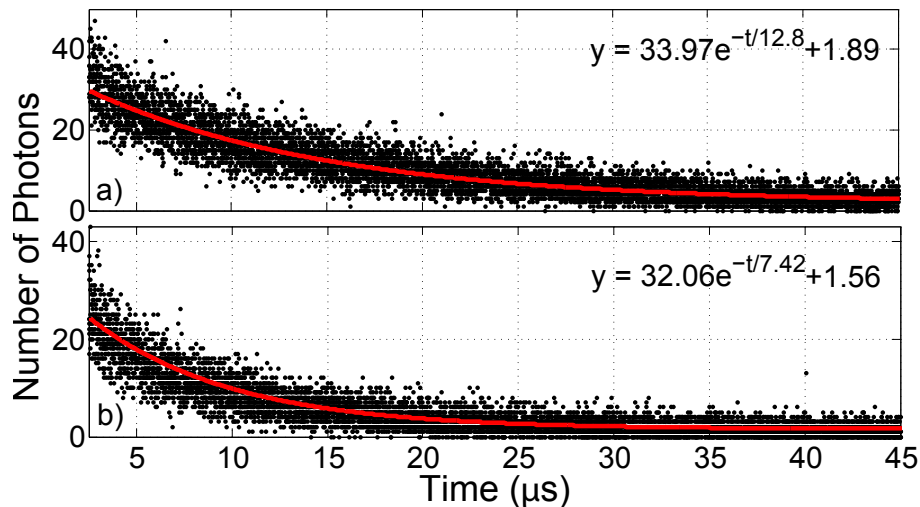


**Fig. 2.** Examples of decays for 5 min integration for glyoxal ((a), 290 ppt<sub>v</sub>) and methylglyoxal ((b), 5400 ppt<sub>v</sub>) taken with the Ti:Sapphire laser with lines of best fit to Eq. (3).

[Title Page](#)[Abstract](#)[Introduction](#)[Conclusions](#)[References](#)[Tables](#)[Figures](#)[⏪](#)[⏩](#)[◀](#)[▶](#)[Back](#)[Close](#)[Full Screen / Esc](#)[Printer-friendly Version](#)[Interactive Discussion](#)

**Quantification of  
gas-phase  
(methyl)glyoxal via  
the LIPGLOS method**

S. B. Henry et al.

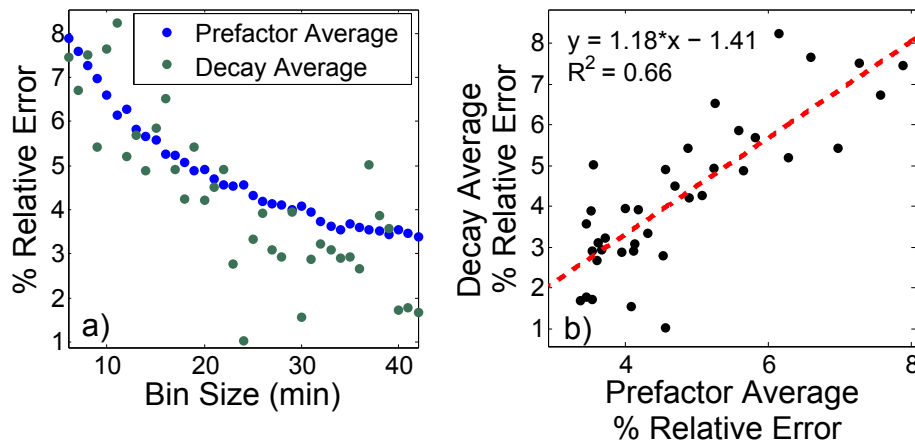


**Fig. 3.** Comparison between the two methods of averaging: prefactor averaging, where the decays of shortest integration are fit followed by averaging the prefactors to desired time resolution, and decay averaging, where the decay is averaged over desired period of integration followed by fitting. **(a)** The percent relative errors for the two averaging methods versus the averaging bin size. **(b)** The correlation between the relative errors in the two averaging methods with the accompanying trend line and equation.

[Title Page](#)[Abstract](#)[Introduction](#)[Conclusions](#)[References](#)[Tables](#)[Figures](#)[⏪](#)[⏩](#)[◀](#)[▶](#)[Back](#)[Close](#)[Full Screen / Esc](#)[Printer-friendly Version](#)[Interactive Discussion](#)

## Quantification of gas-phase (methyl)glyoxal via the LIPGLOS method

S. B. Henry et al.

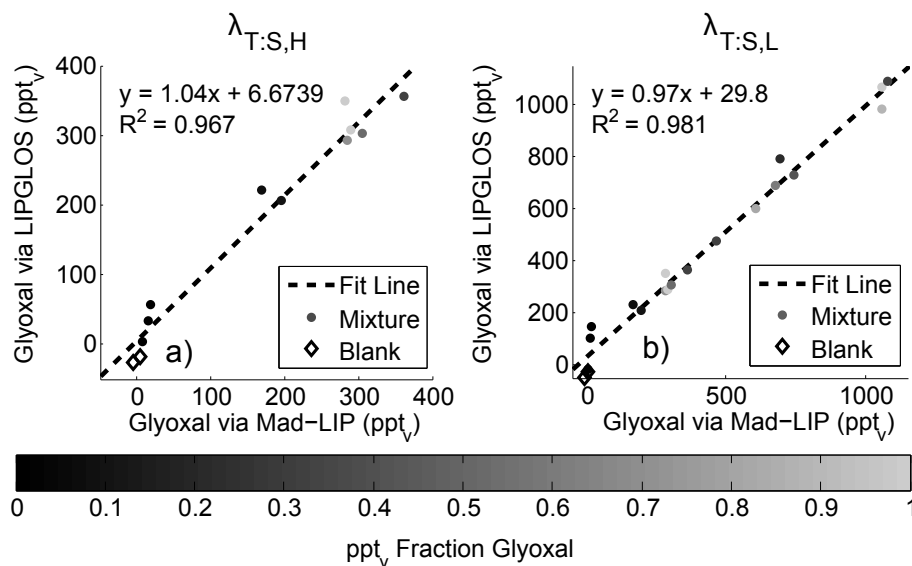


**Fig. 4.** (a) Mixing ratio determined by lifetime method at  $\lambda_{T:S,H}$  versus the Mad-LIP determined concentrations during a simultaneous calibration. (b) Analogous graph for  $\lambda_{T:S,L}$ . The color bar represents the fraction of total glyoxal and methylglyoxal ppt<sub>v</sub> is glyoxal.

Title Page

Abstract

Introduction

Conclusions

References

Tables

Figures

◀

▶

◀

▶

Back

Close

Full Screen / Esc

Printer-friendly Version

Interactive Discussion



---

**Quantification of  
gas-phase  
(methyl)glyoxal via  
the LIPGLOS method**

---

S. B. Henry et al.

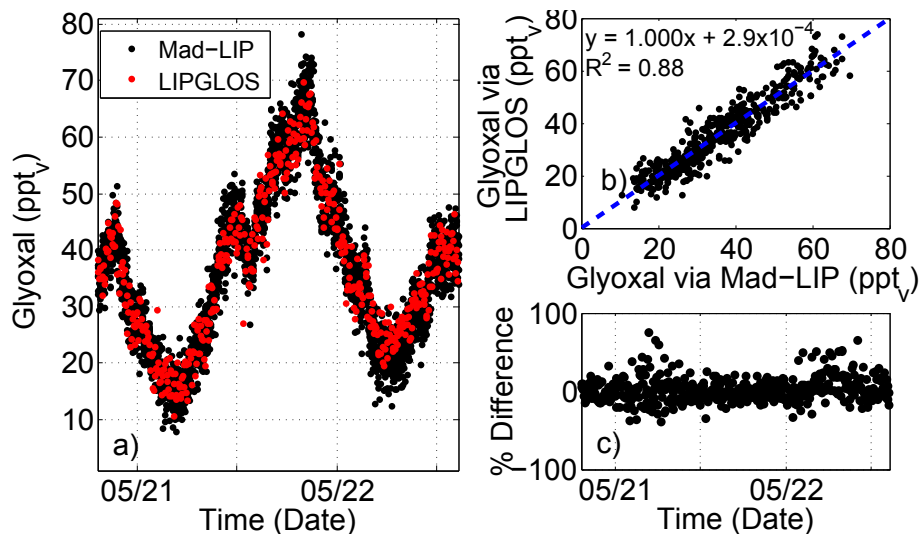


**Fig. 5.** (a) Glyoxal concentration time series from both Mad-LIP (40 s integration) and LIPGLOS (80 s integration). During early morning of the 21st when the concentrations are at their lowest, the standard deviation of the LIPGLOS and Mad-LIP data is 4.2 ppt<sub>v</sub> (extrapolated) and 2.9 ppt<sub>v</sub> in 40 s, respectively. (b) Correlation of measurements coincident within 5 min. (c) Difference between LIPGLOS and Mad-LIP normalized to Mad-LIP measured glyoxal. During the day time hours, the standard deviation of the difference is 8%. During the night, the deviation increases when the noise of the measurement allows values close to zero in the normalization value (glyoxal determined by Mad-LIP).

[Title Page](#)[Abstract](#)[Introduction](#)[Conclusions](#)[References](#)[Tables](#)[Figures](#)[◀](#)[▶](#)[◀](#)[▶](#)[Back](#)[Close](#)[Full Screen / Esc](#)[Printer-friendly Version](#)[Interactive Discussion](#)